Tailoring the optoelectronic properties of BBi alloys: a computational study of $BBi_{1-x}P_x$ and $BBi_{1-x}As_x$

R. Meneceur [a], A. Boukhari [a,*], Y. Megdoud [b, c], L. Tairi[d], Y. Benkrima [e]
[a] *UDERZA Unit, Faculty of Technology, University of El-Oued, Algeria*
[b] *Institute of Sciences, University Center of Tipaza, Algeria*
[c] *LPR Laboratory, Department of Physics, Faculty of Science, Badji Mokhtar University, Annaba, Algeria*
[d] *Research Center in Industrial Technologies CRTI, P.O. Box 64, Cheraga16014 Algiers, Algeria*
[e] *Ecole Normale Superieure de Ouargla 30000 Algeria*

This study conducted on BBi, BP, and BAs, along with their ternary alloys $BBi_{1-x}P_x$ and $BBi_{1-x}As_x$, utilizes the density functional theory. This method is chosen for its ability to accurately assess the fundamental properties of materials. Particularly, the analysis incorporates the (mBJ) Method and the WC-GGA Approximation for correlation potential [37]. Throughout the investigation, the zinc blende phase consistently emerges as the most stable structure. This finding underscores the stability and prevalence of this crystal structure across the studied alloys. The structural parameters exhibit a subtle deviation from linear Vegard's law. Ground state parameters for these materials are found to be in close with both existing theoretical predictions and experimental observations. This agreement ascertains the accuracy of the computational approach used in this study. The study also systematically calculates and analyzes optical properties concerning incident photon energy, and provides insights into how these materials interact with light, which is essential for various applications ranging from optoelectronics to photovoltaics.

(Received Septembre 14, 2024; Accepted January 17, 2025)

Keywords: Phase stability, DFT, mBj, Electronic properties, Optical properties

1. Introduction

Semiconductor Materials (Group III-V) form the cornerstone of numerous commercial technologies and advanced electronic and optoelectronic devices, including transistors, lasers, photodetectors, and frequency-mixing components [1]. These compounds enable the development of multi-junction solar cells with the potential to achieve conversion efficiencies exceeding 40%, making them highly desirable for both space-based and terrestrial applications [2]. The versatility of III–V compounds extend to various industries, from telecommunications to renewable energy [3] due to their exceptional performance and reliability [4]. Advancements in III–V semiconductor technology continue to drive innovation, pushing the boundaries of what's possible in electronics [5], telecommunications [6], and energy harvesting [7]. As research in this field progresses, the integration of III–V compounds into new devices and applications is poised to further revolutionize various industries and improve technological capabilities [8].

Indeed, boron-containing compounds within the III-V semiconductor materials [9] have attracted considerable attention in research due to their remarkable physical characterizations, which distinguish them from other III-V materials. These unique characteristics stem from the distinctive nature of boron atoms, which lack p electrons [10], in their core and possess small atomic sizes [11, 12].

The versatile applications of boron compounds encompass electronic and optoelectronic devices, and photodetectors, showcasing their adaptability in various technological advancements. Beyond electronic applications, boron compounds find utility in industrial settings for purposes like

* Corresponding author: b-amina1@hotmail.fr
https://doi.org/10.15251/DJNB.2025.201.67

cutting/polishing tools and resistant coatings, offering compelling alternatives to materials like diamond due to their exceptional hardness. The growing understanding and exploration of boron compounds open up new avenues for innovation and advancement in both electronic and industrial sectors, contributing to the development of novel materials and technologies.

Theoretical studies on BBi, despite being limited, have provided valuable insights into its potential structural and electronic properties. While experimental synthesis of BBi has not yet been achieved, theoretical predictions offer valuable guidance regarding its properties. Molecular dynamics simulations conducted by Amara et al. [13] shed some light on BBi's behavior, while Ferhat and Zaoui [14] reported a negative bandgap of BBi (-0.085 eV), indicating conflicting findings on its bandgap nature. Various researchers have proposed differing hypotheses regarding BBi's bandgap, with some suggesting an indirect bandgap (Cui and Wang) and others proposing a direct bandgap (Madouri and Yalcin) [15]. The discrepancies in findings highlight the complexity of understanding BBi's properties and underscore the need for further research to elucidate its behavior and potential applications within the III–V semiconductor family.

Cubic boron phosphide (BP) is indeed a binary compound that has garnered attention, particularly in the realm of transferred-electron devices, owing to its unique properties. One of the notable characteristics of BP is its wide bandgap, which is approximately 2 eV. This wide bandgap is advantageous for various electronic and optoelectronic applications [17], facilitating the transmission of sunlight [18]. This study's primary objective is to merge BBi, BAs, and BP compounds to create novel materials, specifically $BBi_{1-x}P_x$ and $BBi_{1-x}As_x$ ternary alloys, with properties falling between those of the individual compounds, thus exploring new avenues for material engineering and application [19-22]. By combining these compounds, researchers aim to harness the unique characteristics of each to develop materials with tailored properties suitable for various electronic, optoelectronic, and industrial applications [23-29].

Our objective is to recalibrate the ground states of BX(X=Bi, As and P) materials, focusing particularly on the equilibrium lattice constant, to better align our results with available experimental data compared to other theoretical studies [20-29]. This recalibration aims to enhance the accuracy of our predictions and ensure that our findings closely match real-world observations. Our investigation covers various aspects, including phase stability, structural, electronic, and optical properties, providing a comprehensive understanding of these materials. By analyzing binary compounds, we aim to validate our approach by comparing our results with both experimental and theoretical findings from the existing literature, ensuring the reliability and relevance of our research.

This article presents a presented the fundamental characterization of ternary alloys $BBi_{1-x}P_x$ and $BBi_{1-x}As_x$, as well as their binary counterparts BBi, BAs, and BP. The investigation offers valuable insights into the fundamental understanding of these materials. The structure of the article is:

Section 1: Introduction: Present the physical properties of the mentioned alloys.

Section 2: Computational Details: This section details the computational methods and techniques employed in the analysis, offering transparency and reproducibility to the research process.

Section 3: Results and Discussions: Presents the findings of the study along with corresponding discussions. This section delves into the implications of the results, highlighting key observations and interpretations.

Section 4: Conclusion: Summarizes the main findings and contributions of the study. It offers insights into the broader implications of the research and potential avenues for further investigation.

By structuring the article in this manner, readers can easily navigate through the research process, from methodology to conclusions.

2. Theoretical details

In this section, we elucidate the computational methodology employed in our study for analyzing the fundamental properties of BBi, BAs, and BP materials, as well as their alloys BBi_{1-}

$_xAs_x$ and $BBi_{1-x}P_x$. The density functional theory (DFT) [30, 31], framework, known for its efficacy in studying electronic structures of materials, was harnessed, utilizing the (FP-LAPW) [32, 33] method. Our calculations were executed within the Wien2k code, a widely used software package for electronic structure calculations. We adopted the generalized gradient approximation (GGA) for exchange and correlation interactions, specifically following the Wu and Cohen (WC-GGA) [35, 36] scheme, to accurately determine total energy and electronic properties. Additionally, to mitigate the well-known GGA underestimation of band gaps, we incorporated the Tran and (mBJ) [37] for electronic property calculations. For the wave function expansion within the atomic sphere, we set the maximum value of angular momentum (l_{max}) to 10. Meanwhile, for the interstitial region, we employed a plane wave expansion with $R_{MT}K_{max}$. A consistent value of seven was chosen for $R_{MT}K_{max}$ across all investigated systems. The Fourier expansion of the potential and charge density utilized $G_{max} = 12\ (R_y)^{1/2}$. Muffin–tin radii (RMT) were assigned specific values: 2.2 a.u. for B, 1.8 a.u. for Bi, and 2.09 a.u. for both P and As. To integrate within the Brillouin zone (BZ), we employed the modified tetrahedron method with a dense mesh of 1000 k-points, ensuring the convergence of total energy to less than 10^{-6} R_y. In conducting ground-state electronic structure calculations, the valence electronic configurations were determined as follows: B - [He] $2s^2 2p^1$, Bi - [Xe] $6s^2 4f^{14} 5d^{10} 6p^3$, As - [Ar] $3d^{10} 4s^2 4p^3$, and P - [Ne] $3s^2 3p^3$.

These computational parameters and methodologies were meticulously selected to provide accurate and reliable insights into the physical properties of the investigated materials.

3. Results interpretation

3.1. Structural characterization

The analysis you've described involves computing the total energies of different crystal structures (Zinc Blend, NaCl, and CsCl) for the selected binary compounds and their ternary alloys across varying volumes. This analysis is crucial for determining the optimized phase stability of the alloys under investigation.

The results, as depicted in Figures 1-3, show the total incident photon (energy) as function a volume curves for the ZB, NaCl, and CsCl phases of the studied materials. These curves provide insights into the relative stability of each crystal structure for the given materials. Based on the graphical representation, it appears that the Zinc Blend (ZB) phase consistently exhibits greater stability compared to the NaCl and CsCl phases across all studied materials. This finding suggests that the ZB structure is the most energetically favorable configuration for the materials under investigation. This information is significant for understanding the preferred crystal structure of the materials and can guide further investigations into their properties and potential applications. It indicates that researchers can focus on studying and optimizing materials with the ZB structure, as it is likely to offer superior stability and performance compared to alternative crystal phases.

Consequently, we employ the Zinc blend structure to derive the ground state characterization of the alloys. It's noteworthy that the system's stability decreases with increasing concentrations of phosphorus and arsenic. Comparatively, the $BBi_{0.5}P_{0.5}$ and $BBi_{0.5}As_{0.5}$ alloy systems exhibit higher stability than the $BBi_{0.25}P_{0.75}$ and $BBi_{0.25}As_{0.75}$ alloy systems but are surpassed in stability by the binary compound. Tracing the general total. The structural properties such as equilibrium lattice constants (a_0) and static bulk modulus (B_0). Murnaghan's equation of state [38] describes the relationship between the total energy of a crystal structure and its volume. Table 1-4 The structural results for the studied materials alongside previous theoretical [39] and experimental works [40].

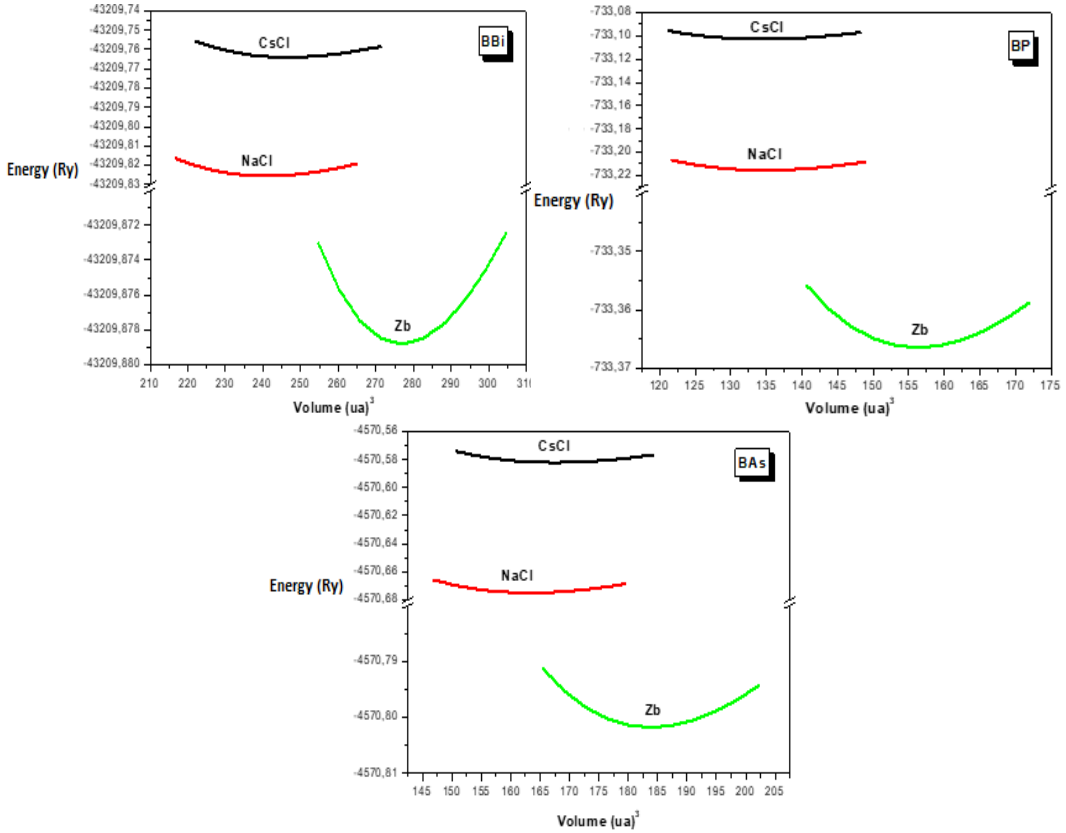

Fig. 1. The variation of the total energy as a function of the volume of BBi, BP and BAs for the concentrations in the ZB, NaCl, CsCl structures.

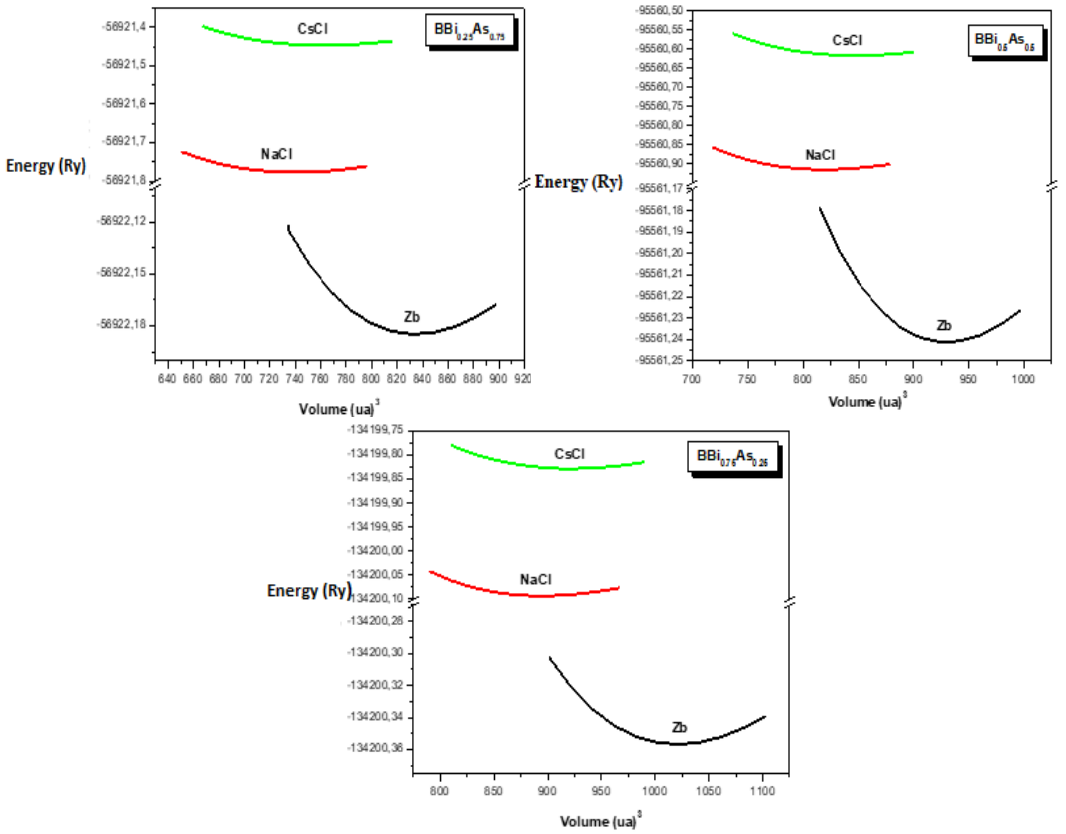

Fig. 2. The variation of the total energy as a function of the volume of $BBi_{1-x}As_x$ for the concentrations x= 0.25, 0.5 and 0.75 in the ZB, NaCl, CsCl structures.

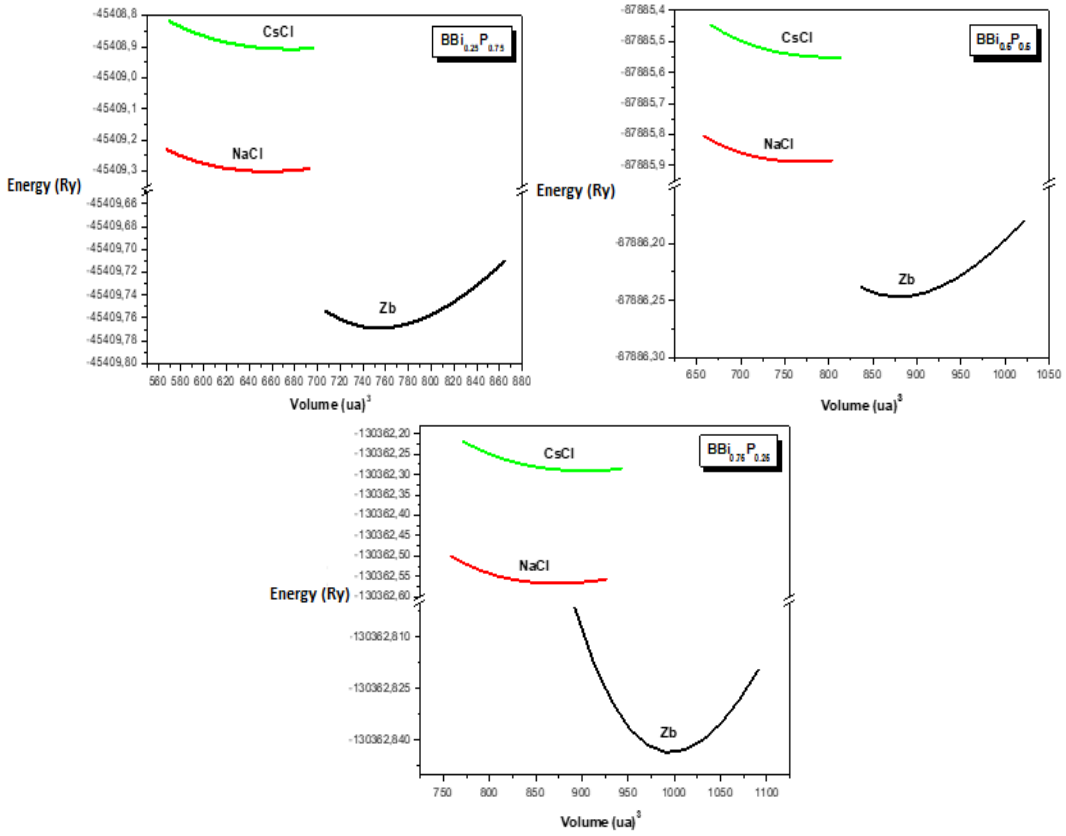

Fig. 3. The variation of the total energy as a function of the volume of $BBi_{1-x}P_x$ for the concentrations x= 0.25, 0.5 and 0.75 in the ZB, NaCl, CsCl structures.

Table 1. The lattice parameters (in Å), the compressibility modulus (in GPa), its derivative for the the compound BBi.

BBi	*a*	*B*	*B'*	*E_0*
NaCl (B1)				
This work	5.226	69.5937	3.8868	-43209.8275
WC-GGA	5.1775	77.7875	4.0590	-43189.1808
LDA	5.3276	61.9762	4.9754	-4333.80208
PBE-GGA	5.22[a]			
Experiment	4.918[b]			
Calculation	5.198[C]			
ZnS (B3)				
This work	5.4754	86.1176	3.7726	-43209.8795
WC-GGA	5.4241	87.6060	3.7709	-43189.2367
LDA	5.3523	6.3763	3.7916	-43343.9602
PBE-GGA	5.392[d]			
Experiment	5.390[e]			
	5.416[f]	83.99[f]	4.36[f]	
Calculation	5.416[h]	86.27[h]	4.6[h]	
	5.529[g]	72.209[g]	4.73[g]	
CsCl (B1)				
This work	3.3176	81.2217	3.897	-43209.7640
WC-GGA	3.2214	83.5897	3.9955	-4356.9845
LDA	3.1987	80.5993	4.0451	-4373.6883
PBE-GGA				
Experiment				
Calculation				

[a]Ref[56], [b]Ref [57], [c]Ref [58], [d]Ref [59], [e]Ref[60], [f]Ref[61], [h]Ref [62].

Table 2. The lattice parameters (in Å), the compressibility modulus (in GPa), its derivative for the different phases considered for the compound BP.

BP	*a*	*B*	*B'*	*E_0*
RS (B1)				
This work				
WC- GGA	4.3069	169.5037	3.9588	-733.2159
LDA	4.2729	177.7375	4.0579	-731.1849
PBE-GGA	4.3276	161.9762	4.2345	-733.8020
Experiment	4.327[a]	155[a]	2.9800[a]	
Calculation	4.320[b]	171[b]	2.82[b]	
	4.339[c]	155[c]		
	4.332[d]	161[d]		
	4.32[j]	156.822[j]		
ZB (B3)				
This work	4.5250	169.1176	3.7726	-733.366
WC-GGA	4.4946	175.6060	3.7709	-731.3366
LDA	4.5523	161.3763	3.7916	-733.9602
PBE-GGA	4.538[e,f,g]	173[e, f, g]		
Experiment	4.558[d]	166[d]	4[d]	
Calculation	4.546[h]	166[h]	3 [h]	
CsCl (B1)				
This work	2.7083	141.7342	3.8937	-733.1026
WC-GGA	2.6865	143.5897	3.1755	731.0687
LDA	2.7238	133.5993	3.436	-733.6883
PBE-GGA				
Experiment				
Calculation				

[a]Ref [63], [b]Ref [64], [c]Ref [65], [d]Ref [66], [e]Ref [67], [f]Ref [68], [g]Ref [69], [h]Ref [70], [i]Ref [71], [j]Ref [72].

Table 3. The lattice parameters (in Å), the compressibility modulus (in GPa), its derivative for the different phases considered for the compound BAs.

BAs	*a*	*B*	*B'*	*E_0*
RS (B1)				
This work	4.5905	135.0548	3.6802	-4570.6757
WC-GGA	4.5502	146.2145	4.1851	-4565.2683
LDA	4.6258	124.4247	3.7659	- 4571.7650
PBE-GGA				
Experiment	4.619[a]	135[a]	3.44[a]	
Calculation	4.583[b]	143[b]		
ZB (B3)				
This work	4.7765	140.0776	4.0496	-4570.8027
WC-GGA	4.8148	131.3025	3.9698	-4571.8985
LDA	4.8135	130.7531	4.3923	-4571.8984
PBE-GGA	4.777[c]			
Experiment	4.77[d, e]	145[d, e]		
	4.726[f]	147[f]	3[f]	
Calculation	4.784[g ,h]	145[g, h]	3[g ,h]	
CsCl (B1)				
This work	2.9170	114.9917	4.3663	-4570.582
WC-GGA	2.8891	123.1169	4.3719	-4565.1700
LDA	2.9409	105.1903	4.7145	-4571.6717
PBE-GGA				
Experiment				
Calculation				

[a]Ref [64], [b]Ref [70], [c]Ref [66], [d]Ref [63], [e]Ref [73], [f]Ref [65], [g]Ref [71], [h]Ref [72].

Tables 4. The lattice parameter a in (A), the compressibility modulus B in (GPa) for the ternary alloys $BBi_{1-x}P_x$ and $BBi_{1-x}As_x$ at different concentrations x.

Alliages	x	Lattice parameters *a*(A)			Compressibility modulus B(GPa)		
		Our results	Exp.	Other calculations WC-GGA	Our results	Exp.	Other calculations WC-GGA
$BBi_{1-x}P_x$	0.25	5.2210	-	5.21623[a]	98.8012	-	99.0604[a]
	0.5	5.0241	-	4.97723[a]	115.7320	-	119.5588[a]
	0.75	4.8434	-	4.7491[a]	139.1442	-	142.5006[a]
$BBi_{1-x}As_x$	0.25	5.3285	-	-	90.5431	-	-
	0.5	5.1648	-	-	100.9934	-	-
	0.75	4.9821	-	-	118.5816	-	-

[a] Ref [75]

Examination of the tables reveals consistent trends: (LDA) Approximation consistently underestimates a_0, while (GGA) Approximation overestimates it. The paragraph mentions that the lattice parameter of BBi obtained using the WC-GGA (weighted-correlation GGA) method is 5.47 Å. This value demonstrates a deviation of approximately 0.99% and 1.07% from the lattice parameters obtained using LDA (5.426 Å) and GGA (5.539 Å), respectively, according to the mentioned reference. [15, 39]. These findings suggest that while BBi has not yet been synthesized experimentally, theoretical calculations, particularly those using the WC-GGA method, provide valuable insights into its structural properties. The consistency of the calculated lattice parameter with previous theoretical works adds credibility to the computational predictions. However, experimental validation of these predictions would be crucial to confirm the accuracy of the theoretical models and further our understanding of BBi's properties and potential applications. The variations in lattice parameters obtained using different methods, such as LDA, GGA, and WC-GGA, are attributed to differences in the parameters used in the calculations, particularly the $R_{MT}K_{MAX}$ values. $R_{MT}K_{MAX}$ refers to the maximum radius of the muffin-tin sphere used in the calculations. In the case of cubic boron phosphide (BP) and boron arsenide (BAs), the WC-GGA method significantly enhances the equilibrium lattice constant (a_0) compared to LDA [40] and GGA [13] schemes. This enhancement leads to lattice parameters that are in excellent close with experimental data. This suggests that the WC-GGA method provides a more accurate description of the structural characterizations of BP and BAs compared to LDA and GGA [40]. These findings establish WC-GGA as highly suitable for the studied materials. Furthermore, the calculated structural parameters for different x value of $BBi_{1-x}Px$ and $BBi_{1-x}As_x$ alloys exhibit a tendency toward Vegard's law [41], characterized by a marginal upward bowing parameter to -0.6976 ($BBi_{1-x}P_x$) and -0.7552 ($BBi_{1-x}As_x$) (Fig. 4). The minor deviation from Vegard's law is mainly attributed to the subtle mismatches in structural phase parameters among the materials BBi, BP, and BAs. It's essential to highlight that the infringement of Vegard's law has been documented in alloys, supported by both experimental observations [41] and theoretical considerations [39]. The overall trend in the variation of the bulk modulus concerning the composition (x) for $BBi_{1-x}P_x$ and $BBi_{1-x}As_x$ alloys is depicted in Fig. 5. When comparing the structural phase constant and bulk modulus of these materials (depicted in Figs. 4 and 5), a consistent pattern emerges: an augmentation of the lattice constant corresponds to a reduction in the bulk modulus.

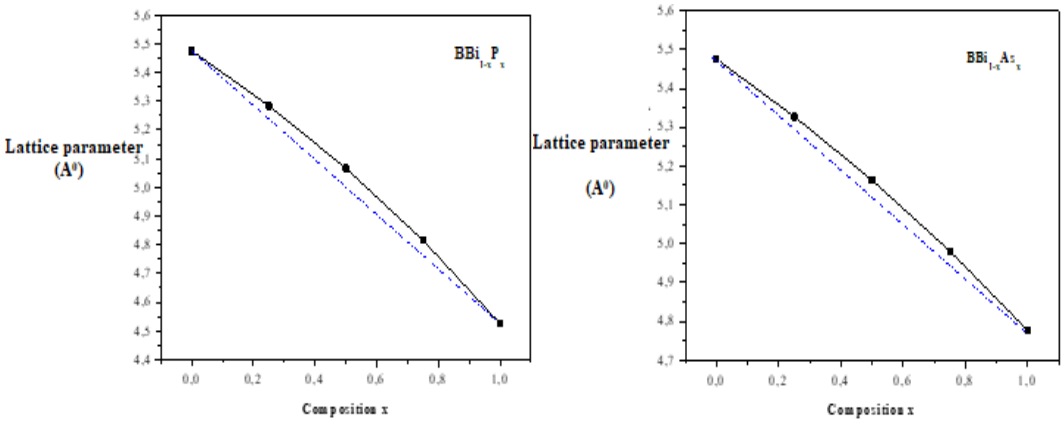

Fig. 4. Variation of the lattice parameter as a function of concentration for $BBi_{1-x}P_x$ and $BBi_{1-x}As_x$ (solid line), compared with that obtained by Vegard's law (dotted line).

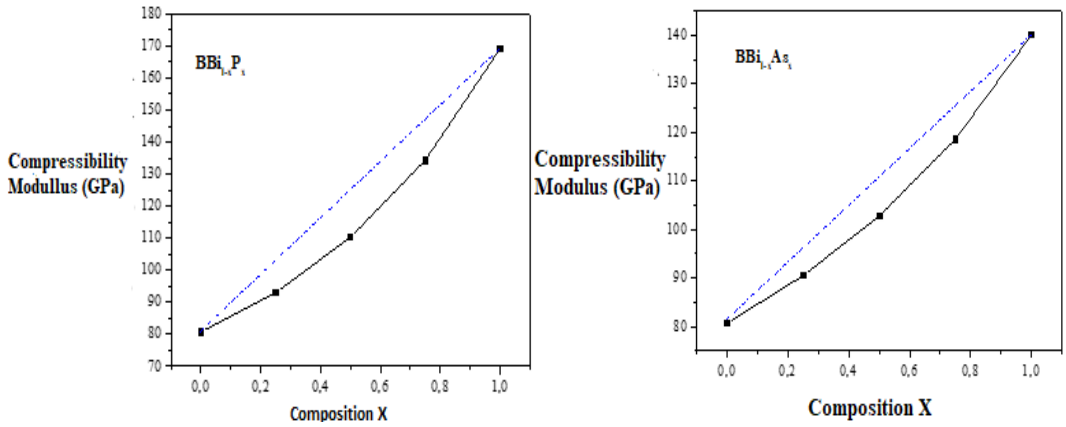

Fig. 5. Variation of the compressibility modulus as a function of concentration for $BBi_{1-x}P_x$ and $BBi_{1-x}As_x$ (solid line), compared with that obtained by the law of linear concentration dependence (dotted line).

3.2. Electronic band structure analysis

The structural electronic bands of the investigated alloys were computed using WC-GGA and mBJ approximations. The mBJ method was specifically applied to present the energy band gaps, while the optimization of the structural phase constant was carried out using the WC-GGA approximation. Initially, the gap energies of the materials BBi, BP, and BAs were determined.

Band structures were computed along high-symmetry directions within the first BZ of a (zinc blende, NaCl, and CsCl). These compounds exhibit bandgap semiconductor behavior, with specific features such as (Γ-Δ_{min}) and (Γ-M) characteristics in zinc blende phase.

Direct band gap phases, known for their excellent optical characterizations, find applications in devices such as light detectors or emitters (e.g., LEDs and lasers) [42-44]. On the contrary, indirect gap structures lack efficient light interaction without heat, leading to disruptions in their electronic properties and resulting in poor electron/phonon-type interactions. Table 5 outlines the diverse band gap values. Notably, for materials in the ZnS stucture, the Interdite-gap value using mBJ aligns closely with theoretical and experimental works [45, 46, 47]. Regarding the material BAs, the interdite-gap obtained through WC-GGA is in proximity to theoretical results. The application of mBJ yields slightly higher band gaps than experimental values [48], but aligns well with specific literature results.

Table 5. Band gap energy Eg (eV) for binary compounds BBi, BAs and BP using the WC-GGA approximation, mBj.

	E_g			
	Present results		Exp.	Other calculations
	WC-GGA	mBj		
BP				
Zinc blende $\Gamma \rightarrow \Delta_{min}$	1.091	1.883	-	1.24[b,d(GGA)], 1.91[b(mBj)], 1.831[g], 1.87[h],
NaCl				1.85[k(mBJ)],
CsCl	1.147[k(WC-GGA)], 1.863[l(mBj)]			
	Métallic	Métallic		
	Métallic	Métallic		
Bas				
Zinc blende $\Gamma \rightarrow \Delta_{min}$	1.223	1.721	1.60[e]	1.21[d(GGA)], 1.25[f], 1.821[g(mBj)], 1,93[c], 1.674[i]
NaCl	1.686[m(mBJ)], 1.092[m]			
CsCl	Métallic	Métallic		
	Métallic	Métallic		
BBi				
Zinc blende	Semi-metal	semi-metal		0.35[a], 0.949[b]
NaCl	and Mettalic[c]			
CsCl	Métallic	Métallic		
	Métallic	Métallic		

[a]Ref [74], [b]Ref [75], [c]Ref [80], [d]Ref [65], [e]Ref[76], [f]Ref[69], [g]Ref [68], [h]Ref [77] , [i]Ref [78], [j]Ref [81], [k]Ref [79],

Table 6. Energy gaps of the ternary alloys $BBi_{1-x}P_x$ and $BBi_{1-x}As_x$.

		Eg (eV)			
		Our results		Exp.	Other calculations
Alliage	x	WC-GGA	mbj		
$BB_{1-x}P_x$	0.25	0.88	1.31		1.08[a]
	0.5	1.13	1.53		0.90[a]
	0.75	1.16	1.77		1.23[a]
$BBi_{1-x}As_x$	0.25	0.35	0.81		
	0.5	0.94	1.45		
	0.75	1.15	1.91		

[a]Ref [75]

The electronic properties of $BBi_{1-x}P_x$ and $BBi_{1-x}As_x$ alloys were studied by analyzing the band structure (Fig. 6) for different concentrations x in the most stable phase (zinc blende). The results obtained are illustred in Table 6. The agreement between the gaps obtained by the mBJ approximation and those calculated experimentally for the binary materials BBi, BAs, and BP reinforces the reliability of the interdit band calculated for the alloys at different concentrations.

$BBi_{1-x}As_x$:

$$E_g^{WC-GGA} = -0.05715 + 2.04354X - 0.76383X^2$$
$$E_g^{mBj} = -0.04898 + 4.16033X - 2.27416X^2$$

$BBi_{1-x}P_x$:

$$E_g^{wc-GGA} = 0.087 + 3.0952X - 2.144X^2$$
$$E_g^{mBj} = 0.11846 + 4.56754X - 2.95314X^2$$

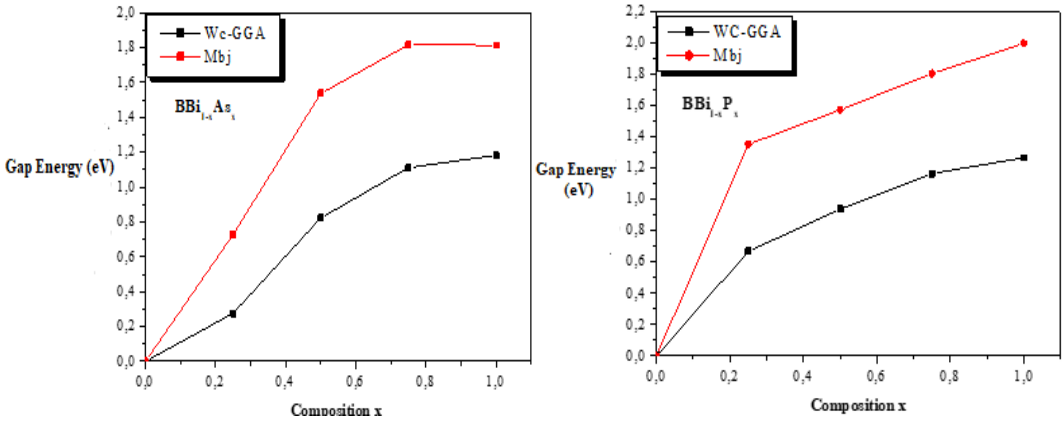

Fig. 6. Variation of the energy gap of the $BBi_{1-x}As_x$ and $BBi_{1-x}P_x$ alloy as a function of the concentration using the WC-GGA and mBj approximations.

The quadratic terms in these equations represent the "disorder parameters" obtained, and they are illustrated in Table 7. These parameters play a crucial role in understanding the electronic characterizations of the alloys. The difference between the values of the lattice parameters of the parent binary compounds and the difference of the electronegativities [49, 50] of the atoms constituting the alloy are the main parameters influencing the nature and the value of the energy deficit.

Table 7. Parameters of disorder b of the alloys $BBi_{1-x}P_x$ and $BBi_{1-x}As_x$ calculated by the Zunger method and by the quadratic adjustment.

		Zunger approach		Qadratic fits	
Alloy	*x*	mBj	WC-GGA	mBj	WC-GGA
$BBi_{1-x}P_x$	b_{VD}	-1.8157	-1.10008		
	b_{CE}	0.346	0.7174		
	b_{SR}	2.765	3.8654		
	b	1.2953	3.48272	-2.9531	-2.144
$BBi_{1-x}As_x$	b_{VD}	-1.20	-0.8328		
	b_{CE}	-4.18	-3.126		
	b_{SR}	3.02	4.9016		
	b	-2.35	-0.6788	-2.2741	- 0.7638

In this methodology, the disorder parameter (b) is:

Volumetric Deformation (bVD): This contribution accounts for the effect of volumetric strain on the energy gaps of the alloys.

Charge Exchange (bCE): The bCE contribution reflects the charge transfer between atoms at the value of the lattice parameter a(x). It quantifies the energy difference between the binary compounds and the alloy due to charge redistribution.

Structural Relaxation (bSR): This contribution measures the change due to structural relaxation, which captures the energy difference between the alloy and its equilibrium lattice parameter. It reflects the change from unrelaxed to relaxed states.

3.3. Optical characterizations

The optical characteristics of a solid are commonly expressed in terms of the complex dielectric function ε(ω), where: $\varepsilon(\omega) = \varepsilon_1(\omega) + i\varepsilon_2(\omega)$ [51].

Here:

$\varepsilon_1(\omega)$: (ω) represents the real part of the dielectric function.

$\varepsilon_2(\omega)$: represents the imaginary part of the dielectric function, associated with the absorption of light and energy dissipation within the material.

The dielectric function provides essential information about how a material interacts with electromagnetic radiation across different frequencies (ω) [52, 53]. It plays a critical role in understanding various optical properties of solids, including absorption, reflection, transmission, and dispersion.

The refractive index of semiconductors holds significant importance as it is a crucial physical parameter linked to microscopic atomic interactions. Additionally, the refractive index n(ω) is intricately connected to the energy band structure of the material. Consequently, several efforts have been made to establish relationships between the refractive index and the energy gap through various models [53, 57].

Commonly employed models include:

Sellmeier Equation: A phenomenological equation that describes the refractive index as a function of wavelength or frequency. It typically involves fitting experimental data to a sum of terms with coefficients called Sellmeier coefficients.

Wemple-DiDomenico Model: This model connects the n(ω) with the interdit band value in semiconductors. It provides a relation between the refractive index and the energy gap based on the complex dielectric function and the energy band structure.

Single Oscillator Model: A simple model that assumes a single electronic oscillator and relates the refractive index to the interdit band value. It provides a straightforward way to understand the optical properties of semiconductors but may lack accuracy for complex materials.

Effective Mass Approximation: In this model, the energy band structure near the band edge is approximated by a parabolic dispersion relation. The refractive index can be related to the effective mass of charge carriers and the energy gap.

These models offer different levels of complexity and accuracy in describing the relationship between the refractive index and the energy gap of semiconductors, making them valuable tools for understanding and predicting optical properties in various semiconductor materials.

The provided description outlines the optical characteristics of various materials, including binary compounds (BX (X= Bi, As and P) and alloy materials ($BBi_{1-x}P_x$ and $BBi_{1-x}As_x$) across different compositions. Here's a summary of the key findings:

3.3.1. The dielectric function ($\varepsilon_1(\omega)$)

The provided information highlights the max peak result of the ($\varepsilon_1(\omega)$) for various materials and compositions. These peak values are indicative of significant optical transitions within the materials and can provide insights into their electronic structure and optical properties.

For the binary compounds: (Fig.7 and 8)

For BBi, the maximum peak result at 1.87 eV.

For BP, the value occurs at 5.71 eV.

For BAs, the value occurs at 5.223 eV.

For the ternary alloy compositions:

For $BBi_{1-x}P_x$ (x=0.25-0.75), the maximum peak values are identified at 2.33, 3.43, and 4.64 eV, respectively.

For $BBi_{1-x}As_x$ (x=0.25-0.75), the maximum peak values occur at 3.613, 4.321, and 5.110 eV, respectively.

These peak values provide important information about the energy levels involved in optical transitions within the materials. By analyzing the dielectric function and its peaks, researchers can gain insights into the materials' electronic band phase, bandgap energies, and optical absorption properties.

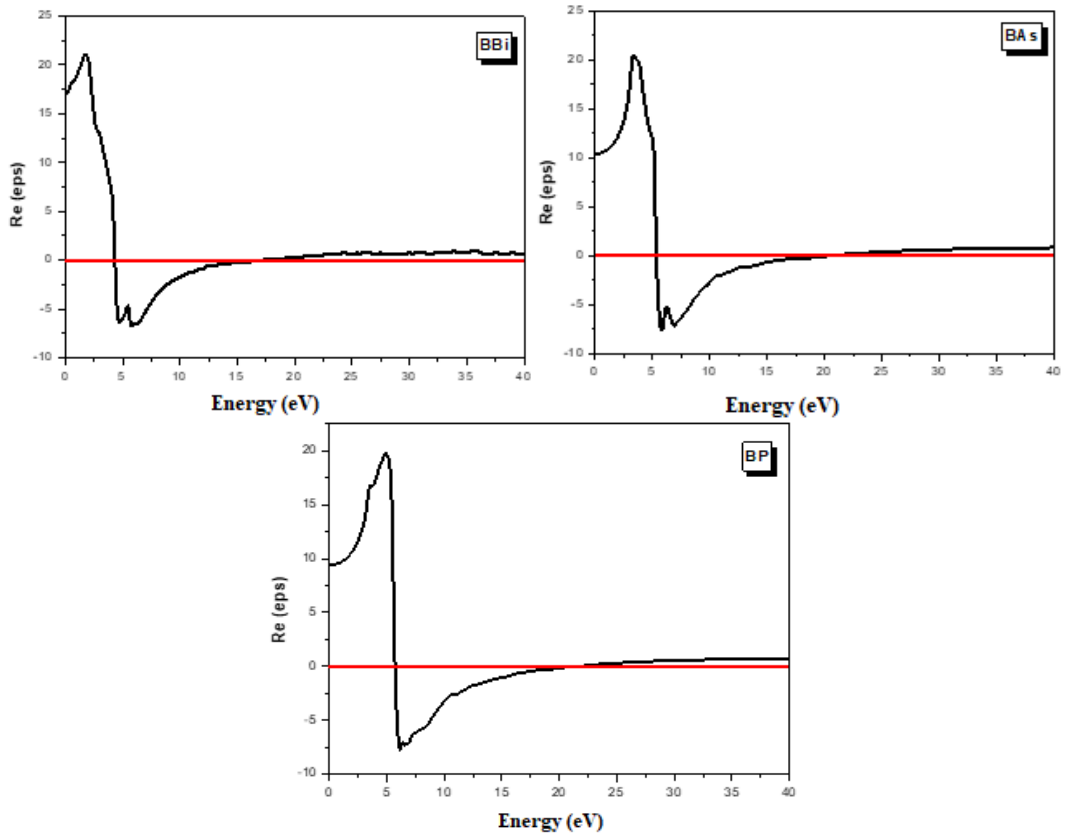

Fig. 7. The variation of the real part of the dielectric function as a function of the energy of the BBi, BAs, BP compounds.

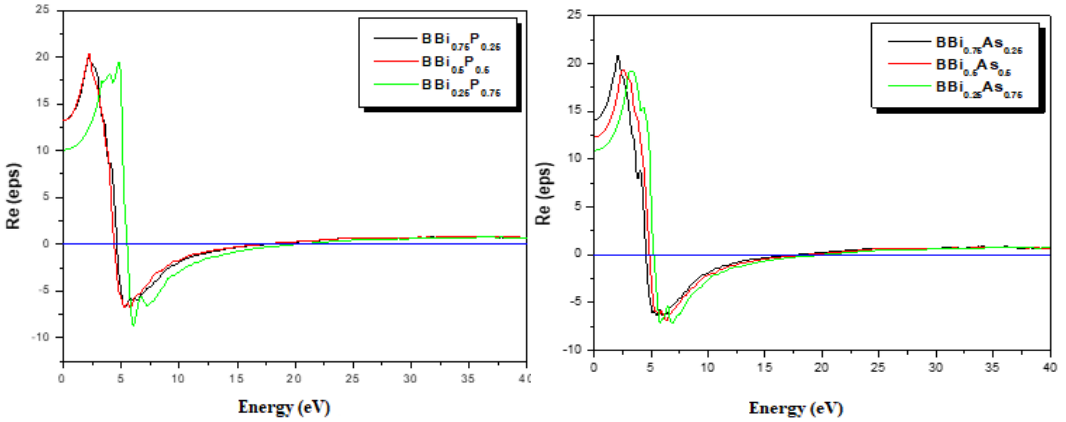

Fig. 8. The variation of the real part of the dielectric function as a function of the energy of the the ternary alloys $BBi_{1-x}Px$ and $BBi_{1-x}As_x$.

3.3.2. The dielectric function ($\varepsilon_2(\omega)$)

The information provided describes additional peaks in the real part of the dielectric function associated with interband transitions, with varying maximum values for different materials and alloys. These peaks are indicative of specific electronic transitions within the materials and provide insights into their electronic band structure and optical properties. (Fig. 9 and 10)

For the binary compounds:

For BBi, the maximum peak value associated with interband transitions occurs at 4.237 eV.

For BP, the maximum peak value occurs at 5.37 eV.

For BAs, the maximum peak value occurs at 5.156 eV.

For the ternary alloy compositions:

For $BBi_{1-x}P_x$ (x=0.25-0.75), additional peak values are found at 4.56, 5.34, and 5.46 eV, respectively.

For $BBi_{1-x}As_x$ (x=0.25-0.75), additional peak values occur at 7.32, 6.43, and 6.22 eV, respectively.

These additional peaks, along with the primary peaks previously mentioned, are associated with transitions involving B 2p states, Bi 6p states, and P and As3p and 4p states. Understanding these interband transitions is essential for characterizing the optical properties of the materials and designing devices based on their optical response.

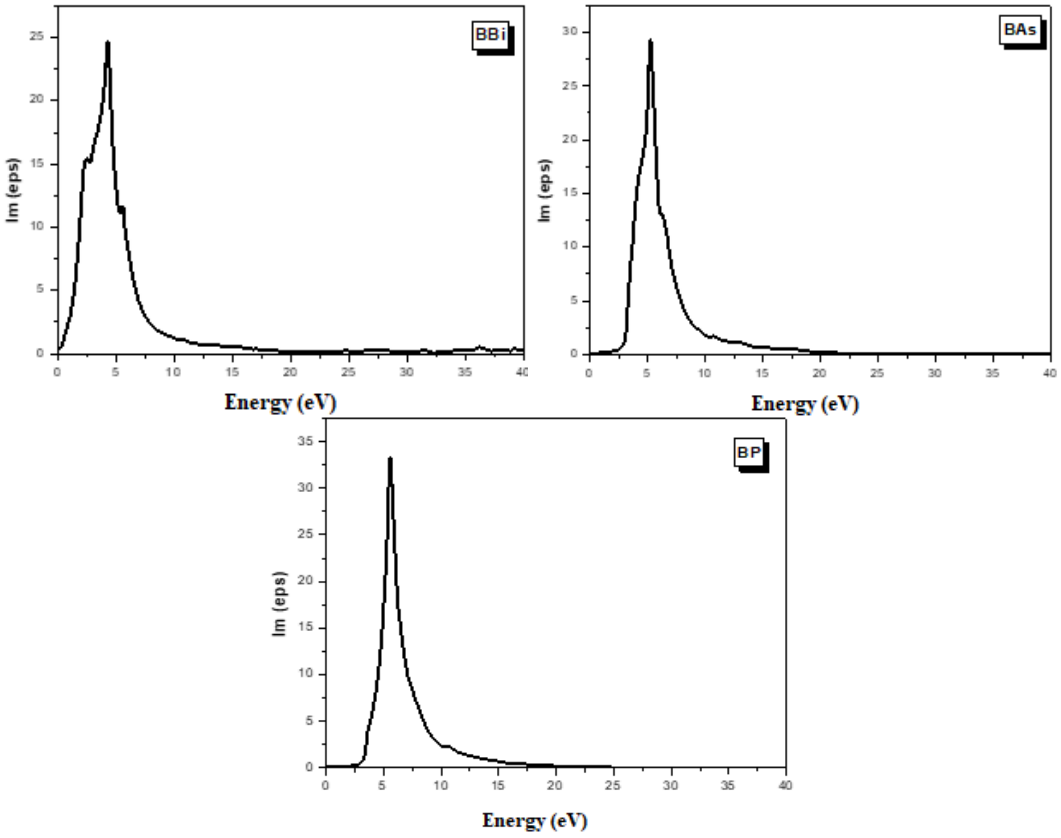

Fig. 9. The variation of the imaginary part of the dielectric function as a function of the energy of the BBi, BAs, BP compounds.

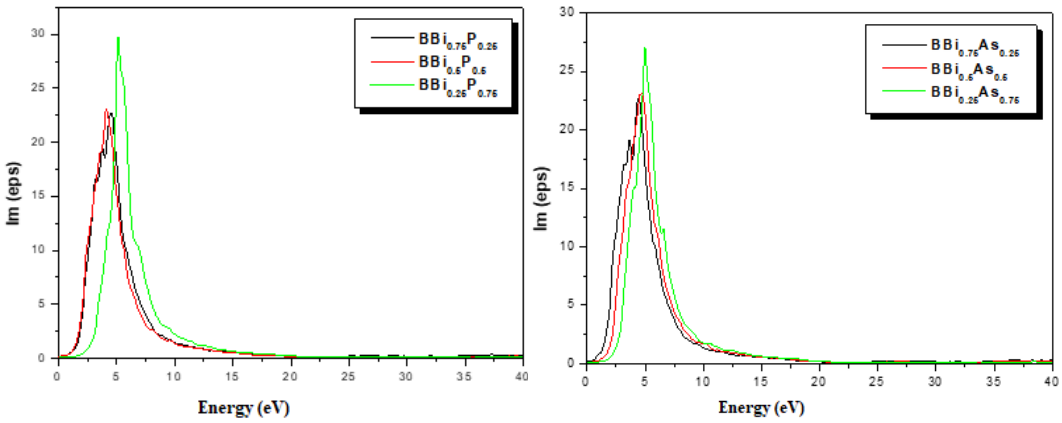

Fig. 10. The variation of the imaginary part of the dielectric function as a function of the energy of the ternary alloys $BBi_{1-x}P_x$ and $BBi_{1-x}As_x$.

3.3.3. Absorption coefficient evolution

The provided information describes the fundamental absorption thresholds and maximal values of the absorption coefficient for each material and alloy, reflecting variations in their optical properties.

For the binary compounds: (For Fig. 11 and 12)

For BBi, the fundamental absorption threshold starts at around 0.041 eV, with a maximal value of the absorption coefficient occurring at 5.879 eV.

For BP, the fundamental absorption threshold starts at around 0.662 eV, with a maximal value of the absorption coefficient occurring at 8.321 eV.

For BAs, the fundamental absorption threshold starts at around 0.975 eV, with a maximal value of the absorption coefficient occurring at 4.541 eV.

For the ternary alloy compositions:

For $BBi_{0.75}P_{0.25}$, $BBi_{0.5}P_{0.5}$, and $BBi_{0.25}P_{0.75}$, the fundamental absorption thresholds start at around 0.683, 0.517, and 0.594 eV, respectively.

For $BBi_{0.75}As_{0.25}$, $BBi_{0.5}As_{0.5}$, and $BBi_{0.25}As_{0.75}$, the fundamental absorption thresholds start at around 0.0334, 0.4567, and 0.6784 eV, respectively.

The maximal values of the absorption coefficient occur at different energy levels for each material and alloy, reflecting their unique optical properties. These energy levels correspond to specific electronic transitions within the materials, providing insights into their electronic band structure and optical response.

Understanding the fundamental absorption thresholds and maximal absorption values is crucial for designing and optimizing materials for various optoelectronic applications, including solar cells, photodetectors, and light-emitting devices. By tailoring the optical properties of materials through compositional adjustments, researchers can enhance their performance in these applications.

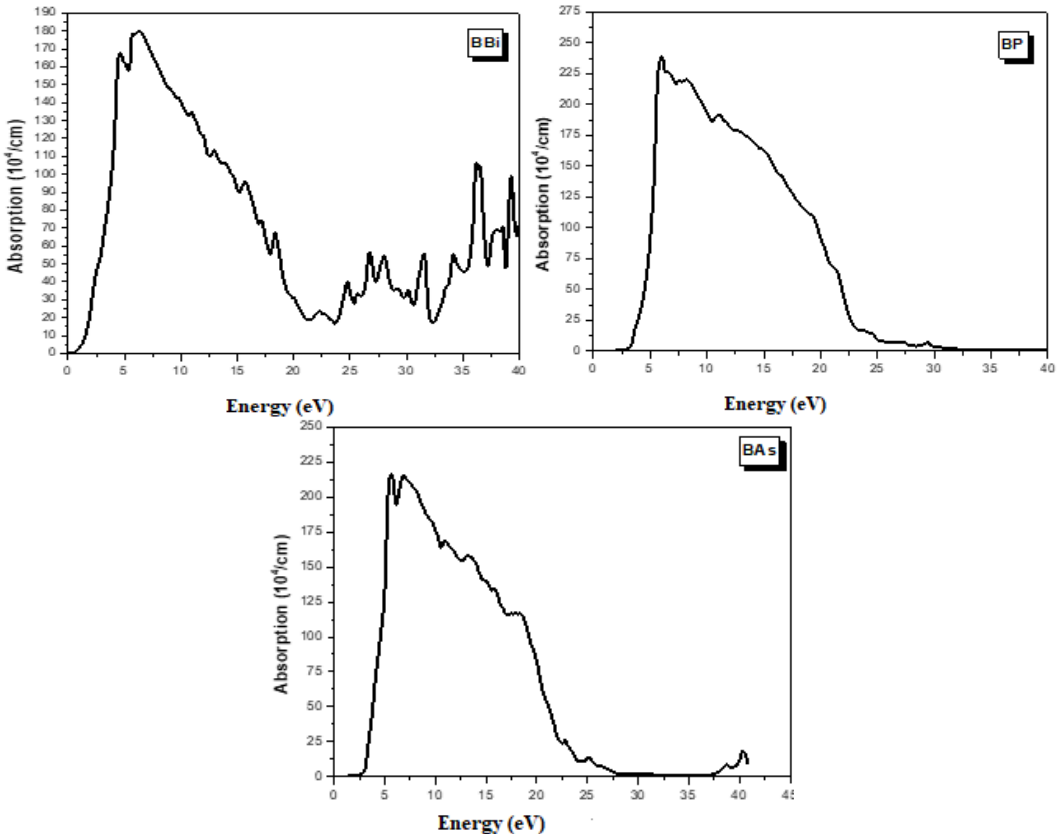

Fig. 11. The variation of the absorption as a function of the energy of BBi, BP and BAs compounds.

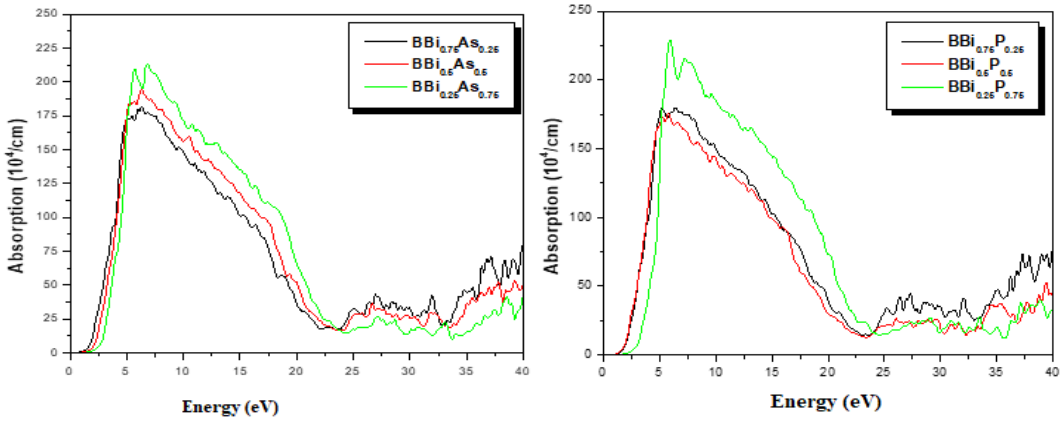

Fig. 12. The variation of the absorption as a function of the energy of ternary alloys $BBi_{1-x}As_x$, $BBi_{1-x}P_x$.

3.3.4. Refractive index (n(ω))

Maximum values of the refractive index are observed at specific energy levels for each material and alloy (Fig.13 and 14). Static values of the dielectric function $\varepsilon_1(0)$ and refractive index n(0) are in agreement with prior theoretical data, considering different approximations. The curves indicate maximum values at the energy levels of 1.401, 1.657, 2.304, 2.697, and 3.713 eV for BBi, $BBi_{0.75}As_{0.25}$, $BBi_{0.5}As_{0.5}$, $BBi_{0.25}As_{0.75}$, and BAs and, 2.301, 2.217, 2.884 and 3.797 eV for $BBi_{0.75}P_{0.25}$, $BBi_{0.5}P_{0.5}$, $BBi_{0.25}P_{0.75}$, and BP, respectively (Table 8 and 9).

Table 8. The dielectric function $\varepsilon_1(0)$ and the refractive index n(0) calculated for the compounds.

	Present results WC-GGA $\varepsilon_1(0)$	Other results	Present results Wc-GGA n(0)	Other results
BP	9.6010	8.12[a]	3.0536	3.33[a]
BBi	22.124		4.6888	
BAs	10.220		3.2188	

[a]Ref [75]

Table 9. The static dielectric function $\varepsilon_1(0)$ and the static refractive index n(0) calculated for the ternary alloys $BBi_{1-x}P_x$ and $BBi_{1-x}As_x$.

	Our results WC-GGA		Other calculations	
Alloy	ε_1	n(0)	ε_1	n(0)
$BBi_{0.75}P_{0.25}$	17.0451	4.2315	12.4[a]	2.23[a]
$BBi_{0.5}P_{0.5}$	12.5533	3.6719	10.7[a]	3.44[a]
$BBi_{0.25}P_{0.75}$	10.3972	3.4313	9.3[a]	4.51[a]
$BBi_{0.75}As_{0.25}$	15.6751	3.9703		
$BBi_{0.5}As_{0.5}$	12.9463	3.6731		
$BBi_{0.25}As_{0.75}$	11.3742	3.3312		

[a]Ref [75]

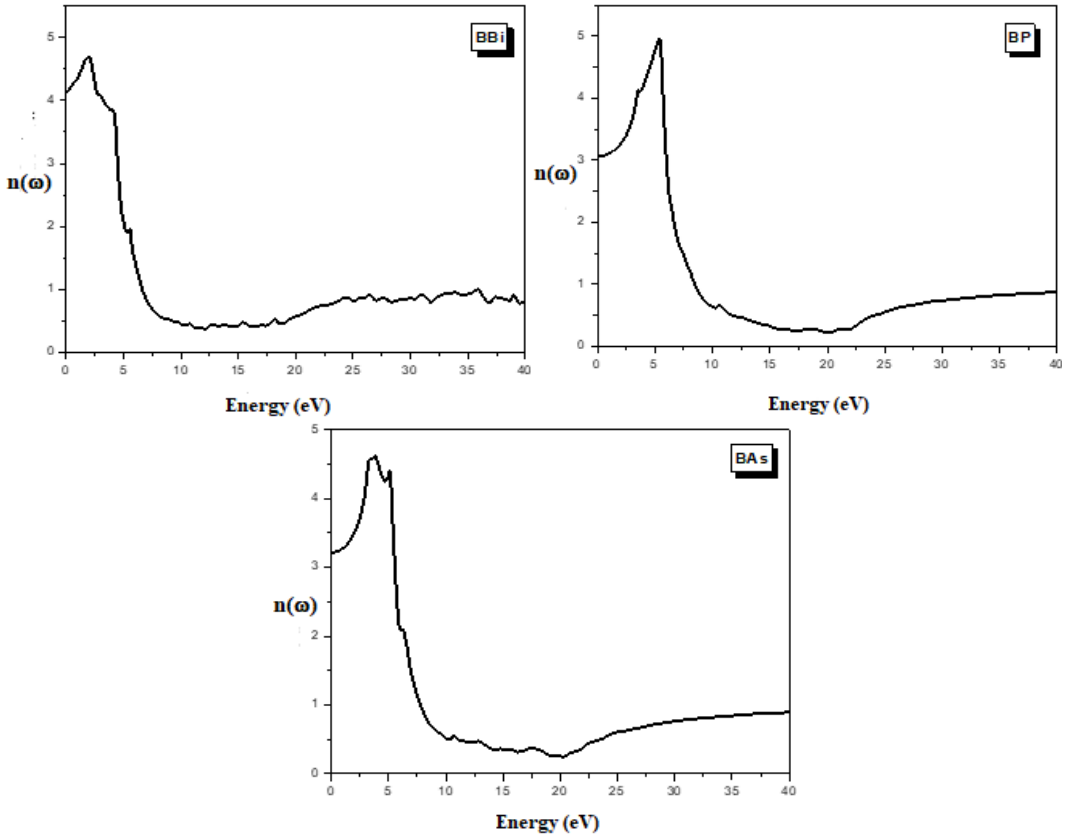

Fig. 13. The variation of the refractive index as a function of the energy of BBi, BP and BAs compounds.

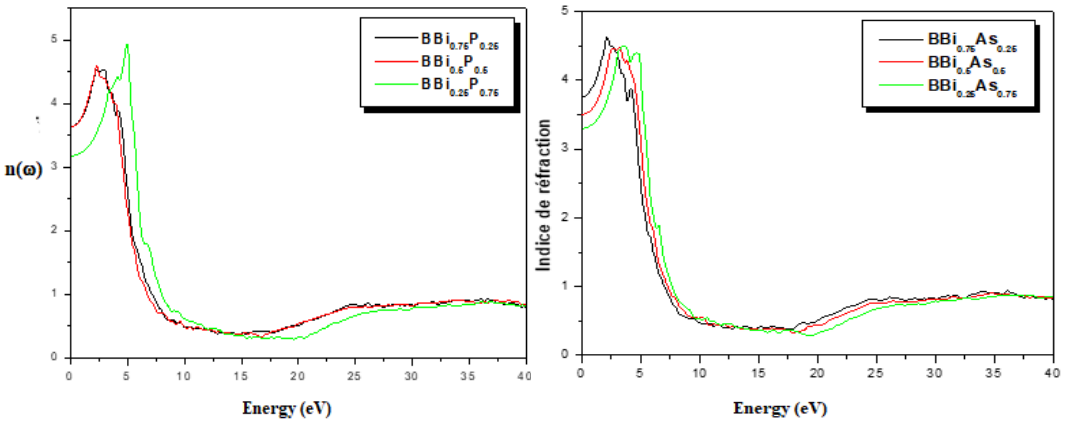

Fig. 14. The variation of the refractive index as a function of the energy of ternary alloys $BBi_{1-x}As_x$, $BBi_{1-x}P_x$.

3.3.5. Reflectivity

Changes in reflectivity across the energy spectrum are depicted, with peak values indicating potential suitability for applications in the infrared range (Fig. 15 and 16). Overall, the analysis provides insights into the optical behavior of the studied materials and alloys, highlighting their potential for various applications in photonics, optoelectronics, and related fields. The curves exhibit peak values of 42% (BBi), 38% ($BBi_{0.75}As_{0.25}$), 32% ($BBi_{0.5}As_{0.5}$), 30% ($BBi_{0.25}As_{0.75}$), 27% (BAs), 25% ($BBi_{0.75}P_{0.25}$), 32% ($BBi_{0.5}P_{0.5}$), 33% ($BBi_{0.25}P_{0.75}$), and 29% (BP).

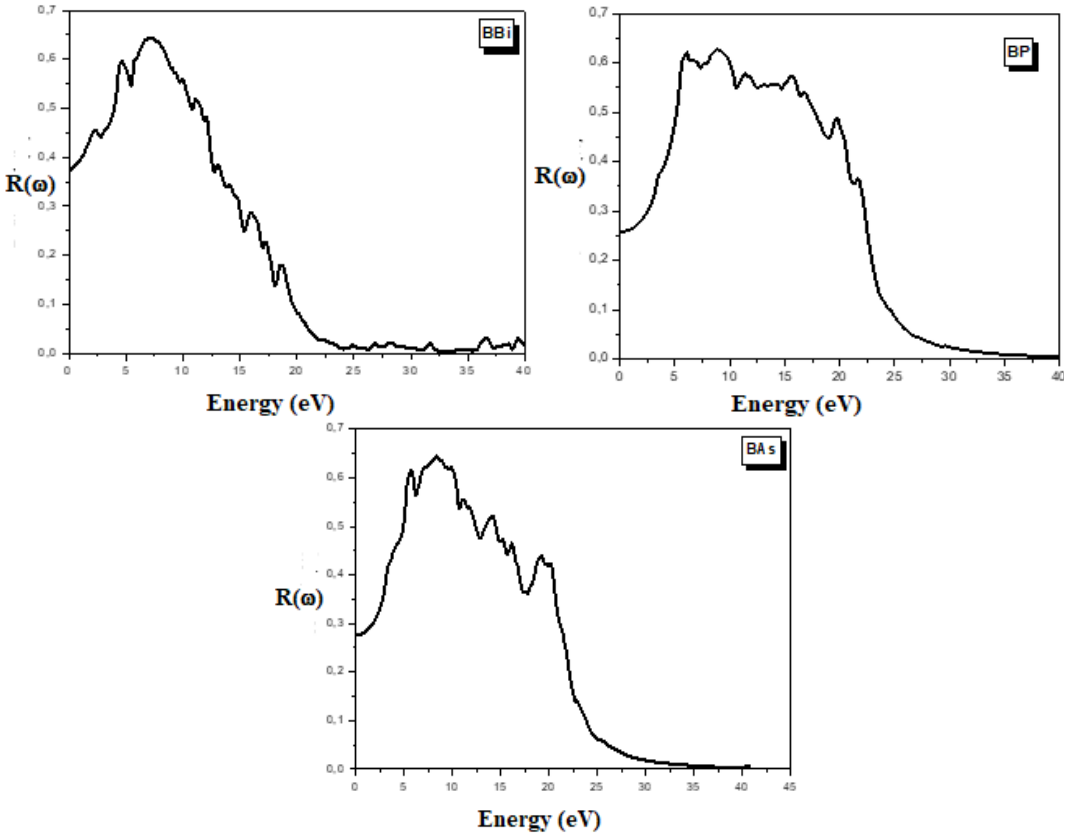

Fig. 15. The variation in reflectivity as a function of the energy of BBi, BP and BAs compounds.

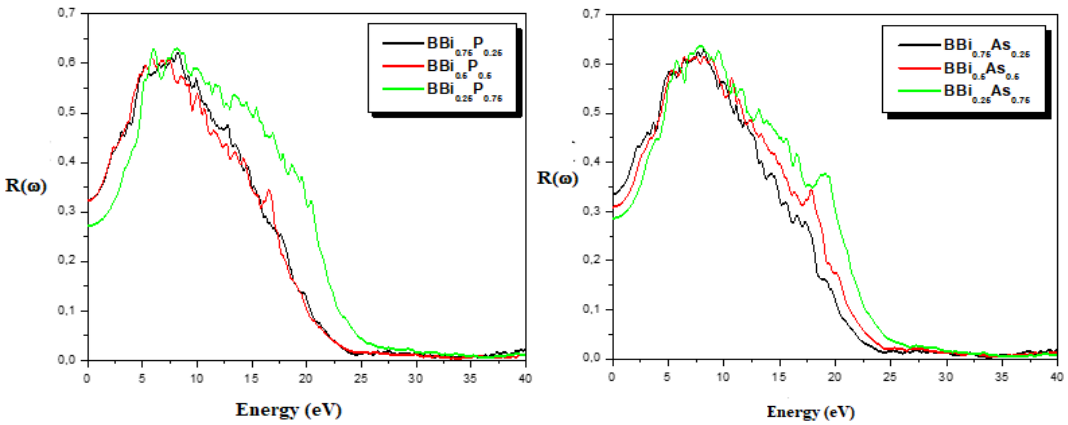

Fig. 16. The variation in reflectivity as a function of the energy of ternary alloys $BBi_{1-x}As_x$, $BBi_{1-x}P_x$.

4. Conclusion

In this work, the fundamental properties of $BBi_{1-x}As_x$ and $BBi_{1-x}P_x$ ternary alloys were thoroughly investigated using the ab-initio method. framework. Here are the key findings and conclusions:

Structural Parameters: The computed lattice parameters and compressibility modulus closely matched both reference values, indicating the reliability of the computational approach.

Electronic Band Structure Analysis: The analysis revealed an indirect band gap for BBi, BAs, and BP, as well as their ternary alloys $BBi_{1-x}As_x$ and $BBi_{1-x}P_x$. The calculated gap values, obtained using both the WC-GGA and mBJ functionals, showed good agreement with existing theoretical data.

Optical Properties: Optical properties, such as the complex dielectric function and refractive index, were investigated. The obtained results were consistent with those derived from other theoretical calculations, further validating the accuracy of the computational method.

In summary, this study provides a comprehensive understanding of $BBi_{1-x}As_x$ and $BBi_{1-x}P_x$ ternary alloys, shedding light on their electronic, optical, and structural behavior. The findings not only confirm the reliability of the computational approach but also contribute to the broader knowledge of these materials, facilitating further exploration and applications in semiconductor technologies.

References

[1] Vurgaftman I., Meyer R., Ram-Mohan L. R., J. Appl. Phys. 89, 5815 (2001); https://doi.org/10.1063/1.1368156

[2] Yamaguchi M., Sol. Energy Mater. Sol. Cells 75, 261 (2003); https://doi.org/10.1016/S0927-0248(02)00168-X

[3] Wentzcovitch R. M., Cohen M. L., Lam P. K., Phys. Rev. B 36, 6058 (1987); https://doi.org/10.1103/PhysRevB.36.6058

[4] Surh M. P., Louie S. G., Cohen M. L., Phys. Rev. B 43, 9126 (1991); https://doi.org/10.1103/PhysRevB.43.9126

[5] Aslan M., Yalcin B. G., Ustundag M., J. Alloys Compd. 519, 55 (2012); https://doi.org/10.1016/j.jallcom.2011.12.020

[6] Wentzcovitch R. M., Chang K. J., Cohen M. L. Phys. Rev. B 34, 1071 (1986); https://doi.org/10.1103/PhysRevB.34.1071

[7] Garcia A., Cohen M. L., Phys. Rev. B 47, 4215 (1993); https://doi.org/10.1103/PhysRevB.47.4215

[8] Golikova O. A., Phys. Status Solidi A 51, 11 (1979); https://doi.org/10.1002/pssa.2210510102

[9] Wentzcovitch R. M., Cohen M. L., J. Phys. C: Solid State. Phys. 19, 6791 (1986); https://doi.org/10.1088/0022-3719/19/34/016

[10] Perri J. A., Laplaca S., Post B., Acta Crystallogr. 11, 310 (1958); https://doi.org/10.1107/S0365110X58000827

[11] Ku S. M. J., Electrochem. Soc. 113, 813 (1966); https://doi.org/10.1149/1.2424125

[12] Chu T. L., Hyslop A. E., J. Appl. Phys. 43, 276 (1972); https://doi.org/10.1063/1.1661106

[13] Ustundag M., Aslan M., Yalcin B. G., Comput. Mater. Sci. 81, 471 (2014); https://doi.org/10.1016/j.commatsci.2013.08.056

[14] Amara K., Soudini B., Rached D., Boudali A., Comput. Mater. Sci. 44, 635 (2008); https://doi.org/10.1016/j.commatsci.2008.04.023

[15] Ferhat M., Zaoui A., Phys. Rev. B 73, 115107 (2006); https://doi.org/10.1103/PhysRevB.73.115107

[16] Cui S., Feng W., Hu H., Feng Z., Wang Y., Comput. Mater. Sci. 47, 968 (2010); https://doi.org/10.1016/j.commatsci.2009.11.030

[17] Wang S. Q., Ye H. Q., Phys. Rev. B 66, 235111 (2002); https://doi.org/10.1103/PhysRevB.66.235111

[18] Madouri D., Ferhat M., Phys. Status Solidi B 242, 285 (2005); https://doi.org/10.1002/pssb.200460029

[19] Yalcin B. G., Bagci S., Ustundag M., Aslan M., Comput. Mater. Sci. 98, 136 (2015); https://doi.org/10.1016/j.commatsci.2014.11.010

[20] Yalcin B. G., Physica B 462, 64 (2015); https://doi.org/10.1016/j.physb.2015.01.021

[21] Lin L., Woods G. T., Callcott T. A., Phys. Rev. B 63, 235107 (2001).

[22] Takigawa M., Satoh J., Shohno K., J. Electrochem. Soc. 122, 824 (1975); https://doi.org/10.1149/1.2134331

[23] Archer R. J., Koyama R. Y., Loebner E. E., Lucas R. C., Phys. Rev. Lett. 12, 538 (1964); https://doi.org/10.1103/PhysRevLett.12.538

[24] Fomichev V. A., Rumsh M. A., J. Phys. Chem. Solids 29, 1015 (1968); https://doi.org/10.1016/0022-3697(68)90237-0

[25] Fomichev V. A., Zhukova I. I., Polushina I. K., J. Phys. Chem. Solids 29, 1025 (1968); https://doi.org/10.1016/0022-3697(68)90238-2

[26] Goossens A., Schoonman J., Electrochim. Acta 40, 1339 (1995); https://doi.org/10.1016/0013-4686(95)00069-Q

[27] Schroten E., Geossens A., Schoonman J., J. Appl. Phys. 83, 1660 (1998); https://doi.org/10.1063/1.366881

[28] Bouhafs B., Aourag H., Cartier M., J. Phys.: Condens. Matter 12, 5655 (2000); https://doi.org/10.1088/0953-8984/12/26/312

[29] Megdoud Y., Mahdjoubi R., Amrani M., Bendjeddou H., Ghemid S., Meradji H., Khenata R., Computational Condensed Matter 22, e00434 (2020); https://doi.org/10.1016/j.cocom.2019.e00434

[30] Hohenberg P., Kohn W., Phys. Rev. B 136, 864 (1964); https://doi.org/10.1103/PhysRev.136.B864

[31] Kohn W., Sham L. J., Phys. Rev. A 140, 1133 (1965); https://doi.org/10.1103/PhysRev.140.A1133

[32] Madsen G. K. H., Blaha P., Schwarz K., Sjostedt E., Nordstr€om L., Phys. Rev. B 64, 195134 (2001); https://doi.org/10.1103/PhysRevB.64.195134

[33] Schwarz K., Blaha P., Madsen G. K. H., Comput. Phys. Commun. 147, 71 (2002); https://doi.org/10.1016/S0010-4655(02)00206-0

[34] Blaha P., Schwarz K., Madsen G. K. H., Kvasnicka D., Luitz J., WIEN2k, An Augmented Plane Wave Plus Local Orbitals Program for Calculating Crystal Properties, Vienna University of Technology, Vienna, Austria, 2001.

[35] Wu Z., Cohen R. E., Phys. Rev. B 73, 235116 (2006); https://doi.org/10.1103/PhysRevB.73.235116

[36] Tran F., Laskowski R., Blaha P., Schwarz K., Phys. Rev. B 75, 115131(2007); https://doi.org/10.1103/PhysRevB.75.115131

[37] Tran F., Blaha P., Phys. Rev. Lett. 102, 226401 (2009); https://doi.org/10.1103/PhysRevLett.102.226401

[38] Murnaghan F. D., Proc. Natl Acad. Sci. USA 30, 244 (1944); https://doi.org/10.1073/pnas.30.9.244

[39] Touat D., Ferhat M., Zaoui A., J. Phys.: Condens. Matter 18, 3647 (2006); https://doi.org/10.1088/0953-8984/18/15/011

[40] Xia H., Xia Q., Ruoff A. L., J. Appl. Phys. 74, 1660 (1993); https://doi.org/10.1063/1.354817

[41] Vegard L. Z., Phys. 5, 17 (1921); https://doi.org/10.1007/BF01349680

[42] Perri J. A., Laplaca S., Post B Acta Crystallography. 11, 310 (1958); https://doi.org/10.1107/S0365110X58000827

[43] Ku S. M., J. Electrochem. Soc. 113, 813 (1966); https://doi.org/10.1149/1.2424125

[44] Geisz J. F., Friedman D. J., Olson J., Kurtz M., Sarah R., Reedy R. C., Swartzlander A. B., Keyes B. M., Norman A. G., Applied Physics Letters 76(11), 1443 (2000); https://doi.org/10.1063/1.126058

[45] Archer R. J., Koyama R. Y., Loebner E. E., Lucas R. C., Phys. Rev. Lett. 12, 538 (1964); https://doi.org/10.1103/PhysRevLett.12.538

[46] Fomichev V. A., Zhukova I. I., Polushina I. K., J. Phys. Chem. Solids 29, 1025 (1968); https://doi.org/10.1016/0022-3697(68)90238-2

[47] Benchehima M., Abid H., Benchikh K., Mater. Chem. Phys. 198, 214 (2017); https://doi.org/10.1016/j.matchemphys.2017.06.009

[48] Tran F., Blaha P., Phys. Rev. Lett. 102, 226401 (2009); https://doi.org/10.1103/PhysRevLett.102.226401

[49] Charifi Z., Baaziz H., Bouarissa N., Int. J. Mod. Phys. B 18, 137 (2004); https://doi.org/10.1142/S0217979204023696

[50] Van Vechten J., Bergstresser T. K., Phys. Rev. Lett. 31, 3354 (1970).

[51] Ravindra N. M. et al., Infrared Phys. Technol. 50, 21 (2007); https://doi.org/10.1016/j.infrared.2006.04.001

[52] Moss T. S., Proc. Phys. Soc. B 63, 167 (1950); https://doi.org/10.1088/0370-1301/63/3/302

[53] Gupta V. P., Ravindra N. M., Phys. Status Solidi B 100, 715 (1980); https://doi.org/10.1002/pssb.2221000240

[54] Ruoff A. L., Mater. Res. Soc. Symp. Proc. 22, 287 (1984).

[55] Reddy R. R. et al., Infrared Phys. 34, 103 (1993); https://doi.org/10.1016/0020-0891(93)90041-5

[56] Deligoz E., Colakoglu K., Ciftci Y. O., Ozisik H., Journal of Physics and Chemistry of Solids 68(4), 482 (2007); https://doi.org/10.1016/j.jpcs.2006.11.021

[57] Daoud S., Lebga N., International Journal of Physical Research 4(1), 1 (2016).

[58] Cui S., Feng W., Hu H., Feng Z., Wang Y., 'First principles studies of phase stability, electronic and elastic properties in BBi compound', Computational Materials Science 4, 968 (2010); https://doi.org/10.1016/j.commatsci.2009.11.030

[59] Bouamama K., Djemia P., Lebga N., Kassali K., High Pressure Research 27(2), 269 (2007); https://doi.org/10.1080/08957950701265359

[60] Ferhat M., Zaoui A., Phys. Rev. B 73, 115107 (2006); https://doi.org/10.1103/PhysRevB.73.115107

[61] Wang S. Q., Ye H. Q., Phys. Rev. B 66, 235111 (2002); https://doi.org/10.1103/PhysRevB.66.235111

[62] Madouri D., Ferhat M., Phys. Status Solidi B 242, 285 (2005); https://doi.org/10.1002/pssb.200460029

[63] Zaoui A., El Haj Hassan F., J. Phys. Condens. Matter 13, 253 (2001); https://doi.org/10.1088/0953-8984/13/2/303

[64] Thakore B. Y., Joshi M. J., Bhatt N. K., Jani A. R., J. Optoelectron. Adv. Mater. 11, 461 (2009).

[65] Wentzcovitch R. M., Cohen M. L., Lam P. K., Phys. Rev. B 36, 6058 (1987); https://doi.org/10.1103/PhysRevB.36.6058

[66] Meradji H., Drablia S., Ghemid S., Belkhir H., Bouhafs B., Tadjer A., Phys. Status Solidi 241 2881 (2004); https://doi.org/10.1002/pssb.200302064

[67] Landolt-Bornstein, in: O. Madelung (Ed.), New Series, Group III, vol. 17a, Springer-Verlag, Berlin, 1982.

[68] Wettling W., Windscheif J., Solid State Commun. 50, 33 (1983); https://doi.org/10.1016/0038-1098(84)90053-X

[69] Knittle R., Wentzcovitch R. M., Jeanloz R., Cohen M. L., Nature 337, 349 (1989); https://doi.org/10.1038/337349a0

[70] Wentzcovitch R. M., Chang K. J., Cohen M. L., Phys. Rev. B 34, 1071 (1986); https://doi.org/10.1103/PhysRevB.34.1071

[71] Hattabi I., Abdiche A., Semari F., Khenata R., Soyalp F., Chin. J. Phys. 56, 2332 (2018); https://doi.org/10.1016/j.cjph.2018.06.025

[72] Ustundag M., Aslan M., Yalcin B. G., Comput. Mater. Sci. 81, 471 (2014); https://doi.org/10.1016/j.commatsci.2013.08.056

[73] Xia H., Xia Q., Ruoff A. L., J. Appl. Phys. 74, 1660 (1993); https://doi.org/10.1063/1.354817

[74] Calabresse E., Fowler W. B., Phys. Status Solidi B 56, 621 (1973); https://doi.org/10.1002/pssb.2220560225

[75] Bagci S., Yalcin B. G., J. Phys. D Appl. Phys. 48, 475304 (2015); https://doi.org/10.1088/0022-3727/48/47/475304

[76] Surh M. P., Louie S. G., Cohen M. L., Phys. Rev. B 43, 9126 (1991); https://doi.org/10.1103/PhysRevB.43.9126

[77] El Haj Hassan F., Akbarzadeh H., Mater. Sci. Eng. 121, 170 (2005); https://doi.org/10.1016/j.mseb.2005.03.019

[78] Buckeridge J., Scanlon D. O., Phys. Rev. Mater. 3, 051601(R) (2019); https://doi.org/10.1103/PhysRevMaterials.3.051601

[79] Benchehima M., Abid H., Comput. Mater. Sci. 14, 114 (2018); https://doi.org/10.1016/j.cocom.2018.01.011

[80] Archer R. J., Koyama R. Y., Loebner E. E., Lucas R. C., Phys. Rev. Lett. 12, 538 (1964); https://doi.org/10.1103/PhysRevLett.12.538

[81] Fomichev V. A., Zhukova I. I., Polushina I. K., J. Phys. Chem. Solids 29, 1025 (1968); https://doi.org/10.1016/0022-3697(68)90238-2